

# Influence of molecular weight on the aggregation-induced emission enhancement and spectral stability of vinyl polymers containing the fluorescent 2,4,6-triphenylpyridine pendant groups†

Chung Tin Lai and Jin Long Hong\*

Received 23rd January 2012, Accepted 5th March 2012

DOI: 10.1039/c2jm30455d

The effect of molecular weight on the aggregation-induced emission enhancement (AIEE) and the spectral stability of vinyl polymers containing fluorescent 2,4,6-triphenylpyridine (TP) pendant groups was evaluated in this study. The high and low molecular weight (MW) vinyl polymers of PDMPS-H and -L are deep-blue emitters with the respective high quantum yields of 82.5 and 84.1% in the solid film state. With high MW ( $M_n = 525,400 \text{ g mol}^{-1}$ ), PDMPS-H also possesses high spectral stability without reduction in the emission intensity upon heating to temperatures above 200 °C. Solutions of the low MW ( $M_n = 37,300 \text{ g mol}^{-1}$ ) PDMPS-L exhibited the normal AIEE effect with continuous emission gains with increasing aggregation upon nonsolvent inclusion. In contrast, the high MW PDMPS-H solutions emitted with constant intensity on all solutions with different extent of aggregation. The emission behavior was then explained by the conformational difference between the PDMPS-L and -H chains and was theoretically approached by computer simulation.

## Introduction

In contrast to the aggregation-caused fluorescence quenching (ACQ)<sup>1–4</sup> observed in the traditional organic fluorophores, the unusual aggregation-induced emission (AIE) or AIE enhancement (AIEE) behavior found in non-coplanar molecules has drawn lots of attention.<sup>5–28</sup> The AIE-operative fluorophores such as the silole (1-methyl-1,2,3,4,5-pentaphenylsilole) molecule emit strongly in the aggregated solution and the solid states, albeit it is nonemissive in the dilute solution state.<sup>5–8</sup> In the aggregated state of silole, the intramolecular rotation (IMR) of the phenyl peripheries against the central silole core was largely restricted, leading to reduced nonradiative decay pathways and the enhanced emission. Due to the advantageous enhanced emissions in the application solid state, lots of organic and polymeric materials with the novel AIE or AIEE properties have been prepared and characterized.<sup>9–39,55</sup>

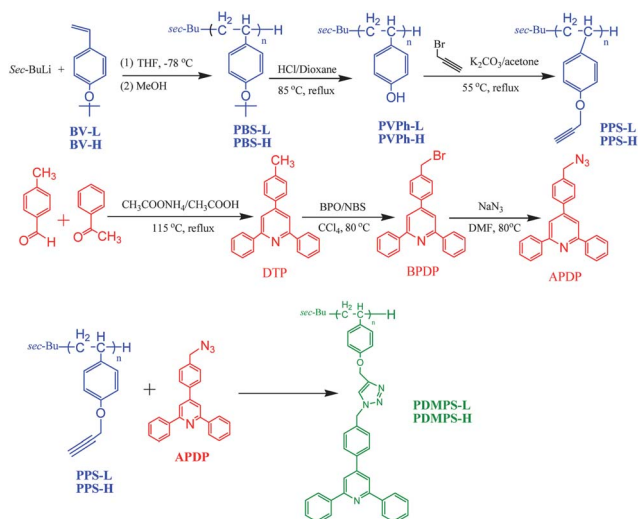
The molecular weight (MW) has been shown to be crucial to the morphology and optoelectronic properties of conjugated polymers such as MEH-PPV,<sup>40–43</sup> polydiacetylene,<sup>44</sup> polythiophenes,<sup>45–47</sup> and polyfluorenes.<sup>48–51</sup> Using the widely-studied MEH-PPV as example, the short MEH-PPV chain exhibits higher diffusion coefficient whereas the long chain MEH-PPV aggregates in the early state. In good solvent, the more extended

MEH-PPV chain tends to assemble into aggregated large nanoparticles with low emission intensity.<sup>42</sup> In the film state, most of the chain segments of high MW MEH-PPV orient in parallel to the film plane, in contrast to the nearly random chain orientation observed in the low MW samples.<sup>43</sup> The chain entanglement as well as thermal and mechanical stabilities generally improved by the high MW also result in less structural defects like aggregates, which are said to be detrimental to emission intensity due to the notorious ACQ effect.<sup>1–4,51</sup>

No previous effort was made to evaluate the effect of MW on AIEE properties. Since the MW of the polymer is closely related to chain mobility and molecular rotation governing the AIE properties, a low and a high MW vinyl polymers (PDMPS-L and -H in Scheme 1) containing novel AIEE-active 2,4,6-triphenylpyridine (TP) pendant fluorophore were prepared to assess the influence of MW on the AIEE-operative emission behavior and the spectral stability at high temperature. The resultant PDMPS-H and -L polymers have distinctive MW difference (with  $M_n = 525,400$  vs.  $37,300 \text{ g mol}^{-1}$ ) and were characterized to be deep-blue emitters with the respective high quantum yields of 82.5 and 84.1% in the solid film states. The high MW PDMPS-H polymer also exhibits high spectral stability without any emission reduction upon heating to temperatures higher than 200 °C. In addition, a DTP molecule (*cf.* Scheme 1) was prepared and used as model compound to probe the AIEE properties of the polymeric analogues. The results also indicated that the PDMPS-H and -L polymers have varied AIEE emission behaviors, which were explained in term of conformational difference between the low and high MW analogues. Theoretical approach for the

Department of Materials and Optoelectronic Science, National Sun Yat-Sen University, Kaohsiung 80424, Taiwan, Republic of China. E-mail: jlhong@mail.nsysu.edu.tw; Tel: +886-7-5252000, ext 4065

† Electronic supplementary information (ESI) available: Fig S1–S10. See DOI: 10.1039/c2jm30455d



**Scheme 1** Preparation of polymeric PPS-L and -H and small-mass APDP and their further click reaction to yield the desired PDMPs-L and -H products.

single-chain conformation was manoeuvred by computer simulation, along with it, the  $^1\text{H}$  NMR, fluorescence (FL) spectra, dynamic light scattering, rheology and viscosity measurements were all used to evaluate plausible reasons leading to the varied emissive behaviors and spectral stability between the low and the high MW PDMPs.

## Results and discussion

### Synthesis

The vinyl polymers PDMPs-L and -H with the AIE-active TP pendant group were prepared by the facile click reaction between the azide-functionalized APDP molecule and the polymeric PPS (PPS-L and -H) with acetylene pendant groups (Scheme 1). To have the polymeric PPS-L or -H, the required poly(*t*-butoxy styrene)s of low and high molecular weights (PBS-L and -H) were prepared by the anionic polymerization with controlled monomer/initiator (BV/*sec*-BuLi) ratio. The *t*-butoxy groups in the PBS polymers were then hydrolyzed by HCl to generate the hydroxyl (–OH) group in the resultant PVPPhs, which were then reacted with propargyl bromide to generate the desired acetylene pendant functions in PPSs. As another reactant for the click reaction, the azide-functionalized APDP was prepared from a three-step reaction procedures starting from the DTP molecule, which was synthesized from the Chichibabin reaction between *p*-tolualdehyde and acetophenone in 1 : 2 molar ratio and was used as model compound to simulate the emission behavior of the polymeric PDMPs. The 4-methyl group in DTP was then reacted with NBS to yield the desired bromomethyl function, which under the attack of  $\text{NaN}_3$  was transformed into the azide group in the desired APDP compound, of the intermediate BPDP compound. The chemical structures of all organic intermediates and products were carefully characterized and confirmed by the  $^1\text{H}$  NMR, infrared and mass spectroscopy and elemental analysis.

Molecular weights of all polymeric materials were evaluated from the GPC analysis (Fig. S5, ESI $^\dagger$ ) and the results were

summarized in Table 1. GPC analysis indicated that the starting polymers PBS-L and -H from the controlled living anionic polymerizations have narrow PDIs (1.08 for PBS-L and 1.06 for PBS-H). Further chemical transformations of the *t*-butoxy group proceeded to resulted in the final PDMPs products. The PDMPs-H has a higher  $M_n$  ( $= 525,400 \text{ g mol}^{-1}$ ) and  $M_w$  ( $= 583,200 \text{ g mol}^{-1}$ ) than those for PDMPs-L ( $M_n = 37,300 \text{ g mol}^{-1}$ ,  $M_w = 42,200 \text{ g mol}^{-1}$ ). The large MW difference between PDMPs-H and -L resulted in the differences in the corresponding emission and thermal properties, points will be discussed later.

The efficient transformation from hydroxyl to acetylene pendant functions<sup>52</sup> and the success on the click reaction<sup>53,54</sup> can be demonstrated by  $^1\text{H}$  NMR spectra. Substitution level of PDMPs depends on the the starting PVPPh and the following click reaction between APDP and PPS. Degrees of conversions to acetylene functions in PPS-L and PPS-H are 99.1% and 98.2, respectively, which can be calculated from the integration ratios between the proton  $\text{H}_d$  ( $-\text{CH}_2-\text{C}\equiv\text{C}-$ ) and protons  $\text{H}_{e,f}$  (aromatic Hs) in the  $^1\text{H}$  NMR spectra (Fig. 1). The efficiency of the click reaction can be also assured from the  $^1\text{H}$  NMR spectra: the methylene  $-\text{CH}_2-\text{N}_3^+$  resonance (4.25 ppm, proton **a** in Fig. S3, ESI $^\dagger$ ) of APDP and the methylene  $-\text{CH}_2-\text{C}\equiv\text{C}-$  resonance (4.7 ppm, proton **d** in Fig. 1) of PPS are no longer observed in the spectra of the PDMPs products (Fig. 2). Instead, the two methylene resonances (protons **c** and **d**) for PDMPs appear at 5.1 and 5.6 ppm, respectively. Conversions of PDMPs-L and -H thus evaluated are 99.7 and 99.1, respectively. The aromatic resonances (protons **g–k**) for the TP fluorophores in PDMPs-L and -H are virtually different in shape, comment will be given later in this discussion.

Infrared spectra in Fig. S4 (ESI $^\dagger$ ) can be conveniently used to demonstrate the success of the functional group transformations. The large hydroxy stretching band (in the ranges of 3000 to 3600  $\text{cm}^{-1}$ ) of PVPPh-L (or –H) was replaced by the sharp acetylenic  $-\text{C}\equiv\text{C}-\text{H}$  stretching at 3288  $\text{cm}^{-1}$  in the spectrum of PPS-L (or –H), which indicates that conversion from the hydroxy  $-\text{OH}$  to the propynoxy  $-\text{O}-\text{CH}_2-\text{C}\equiv\text{C}-\text{H}$  group proceeded quantitatively. Successful click reaction can be demonstrated from the result that the azide  $-\text{N}_3^+$  (2100  $\text{cm}^{-1}$ ) stretching of APDP and the acetylenic  $-\text{C}\equiv\text{C}-$  (2120  $\text{cm}^{-1}$ ) stretching of PPSs were almost absent in the spectra of the final PDMPs products.

**Table 1** Molecular weights determined from GPC

Sample	PBS-L	PBS-H	PVPPh-L	PVPPh-H
$M_n$ ( $\text{g mol}^{-1}$ ) <sup>a</sup>	16,000	209,000	10,600	153,500
$M_w$ ( $\text{g mol}^{-1}$ ) <sup>b</sup>	17,300	221,600	11,300	161,200
PDI <sup>c</sup>	1.08	1.06	1.06	1.05
Sample	PPS-L	PPS-H	PDMPs-L	PDMPs-H
$M_n$ ( $\text{g mol}^{-1}$ ) <sup>a</sup>	14,500	195,100	37,300	525,400
$M_w$ ( $\text{g mol}^{-1}$ ) <sup>b</sup>	15,800	208,800	42,200	583,200
PDI <sup>c</sup>	1.09	1.07	1.13	1.11

<sup>a</sup> Number-average molecular weight,  $\text{g mol}^{-1}$ . <sup>b</sup> Weight-average molecular weight,  $\text{g mol}^{-1}$ . <sup>c</sup> Polydispersity.

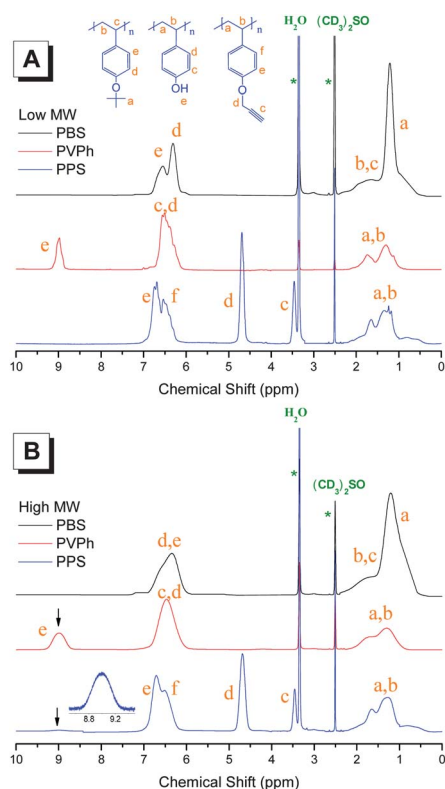


Fig. 1  $^1\text{H}$  NMR spectrum of PBS, PVPh and PPS ( $\text{DMSO}-d_6$ ).

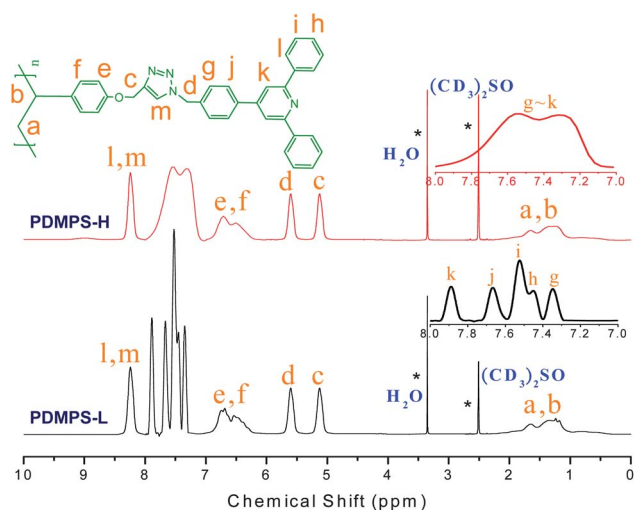


Fig. 2  $^1\text{H}$  NMR spectrum of PDMP-S-L and PDMP-S-H solutions ( $10^{-3}$  M). ( $\text{DMSO}-d_6$ ).

The MW difference between the low and high MW polymeric intermediates and products resulted in the respective low and high glass transition temperatures ( $T_g$ s) shown in the DSC thermograms (Fig. 3). With higher MWs, the high MW PBS-H, PVPh-H, PPS-H and PDMP-S-H all have higher  $T_g$ s than their low MW analogues. The final PDMP-S-H product has a high  $T_g$  of 211 °C, which is 51 °C higher than the resolved 160 °C for the PDMP-S-L counterpart. Except the distinct  $T_g$  difference, polymers PDMP-S-L and -H also showed varied FL emission behaviors in the solution and in the solid states.

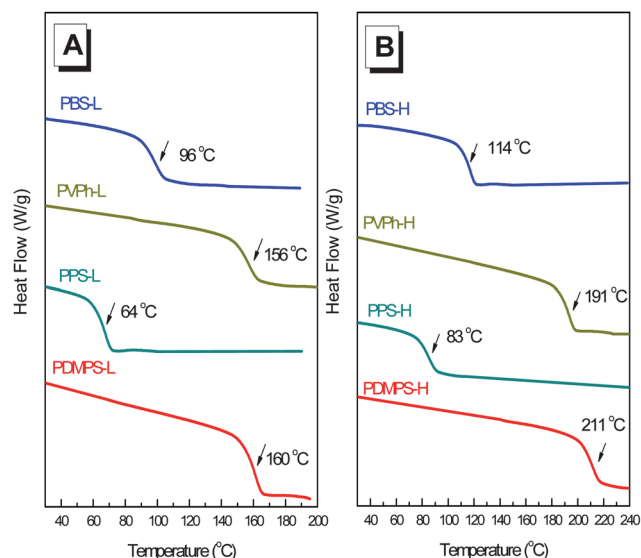


Fig. 3 DSC thermograms of (A) low MW and (B) high MW polymers of PBS, PVPh, PPS and PDMP-S.

#### Emission behavior of DTP, PDMP-S-L and -H solutions

The small-mass model DTP was studied first, as shown in Fig. 4A, dilute ( $10^{-5}$  M) solution of DTP in THF is essentially nonemissive but with the gradual inclusion of water nonsolvent the FL emissions become more intense. The operative AIE effect can be better illustrated by the increasing quantum yield ( $\Phi_F$ ) upon increasing water content in the solutions; the summarized results in Fig. 4B suggest that a maximum  $\Phi_F$  value of 32% can be reached when the water content in the solution is 60 vol%, however, further increase of water content resulted in no emission gain as seen from the constant  $\Phi_F$ s for solutions with water content  $\geq 60$  vol%. The solution FL emission spectra in Fig. 4A contain a long-wavelength tail extended over 400 nm while in the

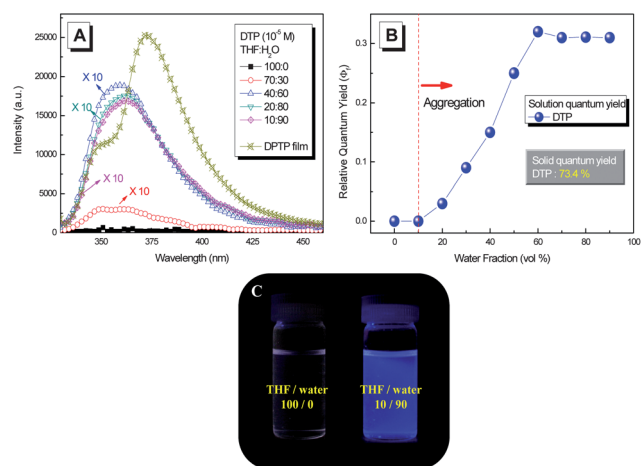


Fig. 4 (A) FL emission spectra of solid film and dilute ( $10^{-5}$  M) solution of DTP in THF/water solvent mixtures of varied compositions, (B) the summarized solution quantum yield ( $\Phi_F$ ) vs. solution composition (inset: solid quantum yield), and (C) photographs of DTP in pure THF (left) and THF/water mixture (90% volume fractions of water) (right) under illumination with a 365 nm UV lamp.

solid state a strong emission band (at 372 nm) separated from the monomer emission was observed. Recently, pyrene-substituted ethenes (PSEs)<sup>55</sup> were reported to exhibit aggregate-enhanced excimer emission with strong long-wavelength excimer emission due to the inherent  $\pi$ - $\pi$  intermolecular interactions and multiple hydrogen bonds. Similar emission response between PSEs and DTP molecules indicated that excimer formation is the possible source for the strong emission at 372 nm. The enhanced excimer formation in the solid state contributed to the high  $\Phi_F$  of 73.4%, comparatively higher than those of the solution samples.

The solution emission behavior of the polymeric PDMPS-L in THF/water characterized its AIEE effect; as shown in Fig. 5A, the weakly-emissive solution of PDMPS-L in pure THF gradually gained emission intensity as the water content in the solution increased. Although weak in intensity, solution of PDMPS-L in THF did emit with the discernible monomer and aggregate emission bands at 350 and 372 nm, respectively. With increasing water inclusion, the monomer emission merged with the strong aggregate emission and the large emission gain here is actually due to the strong aggregate emission, which suggests that the developed aggregates upon water addition maximized the observed AIEE effect. Aggregate development resulted in the bathochromic shift of the aggregate peak from 372 to 383 nm. Further aggregation on the solid sample resulted in a spectrum containing mostly the aggregate emission band centered at a wavelength (389 nm) longer than the aggregate solutions. The emission enhancement can be also verified from the summarized  $\Phi_F$ s in Fig. 5B. The resultant  $\Phi_F$  values (25–78%) for the PDMPS-L mixture solutions are comparatively higher than those (0–32%) of the DTP solutions; therefore, extent of aggregation is expected to be higher in the polymer as compared to the small-mass DTP. High extent of aggregation on the solid PDMPS-L also led to further increase of  $\Phi_F$  to a high value of 84.1%.

The solution emission of the high MW PDMPS-H is different from the low MW analogue in two aspects; firstly, there existed

only a small emission difference between 0 and 60 vol% water solutions (Fig. 6A). Secondly, all emission spectra contained mainly the long-wavelength aggregate emission with little peak shifts from 375 to 380 nm. The emission spectrum of the solid PDMPS-H also resembles the solution ones, which may indicate the extent of aggregation in the mixture solutions and the solid sample are quite the same and indeed, the resultant  $\Phi_F$ s are all in the vicinity of 82 to 84% (Fig. 6B) for the aggregated solutions and the solid samples. From the resolved  $\Phi_F$ s, the PDMPS-H chains in the mixture solutions have higher degrees of aggregation than the PDMPS-L chains in solutions; however, little difference exists in the solid samples in view of their  $\Phi_F$ s (82.5 vs. 84.1%).

Emissions of dilute solutions ( $10^{-5}$  M) of DTP, PTMPS-L and -H in THF at varied reduced temperatures were then measured. The maximum peak intensity summarized in Fig. 7 indicates the large emission enhancements of the DTP and the PTMPS-L solutions with decreasing temperature (before the freezing point of the mixture solution at  $-108$  °C), which is in distinct contrast to the small emission gain of the PTMPS-H solution during the cooling cycle. The insensitivity of the PDMPS-H solution toward cooling suggests that the long polymer chain of PDMPS-H at room temperature already imposed high energy barriers for the molecular rotations of the pendant TP fluorophores and therefore, cooling did not much alter the rotation energy barrier leading to effective nonradiative decay pathways. On the other hand, the molecular rotations of the TP fluorophores in the small-mass DTP and the low MW PDMPS-L are considered to proceed readily due to their less segmental constraints. The high MW of the PDMPS-H chain should impose high energy barrier for free molecular rotation and we will discuss it later. With the lower rotation barriers, TP fluorophores in DTP and PDMPS-L underwent active molecular rotations and cooling did exert effectively in preventing facile molecular rotations leading to nonradiative decay process. At temperatures  $<-108$  °C (close to the freezing point of mixture solutions), serious scattering from

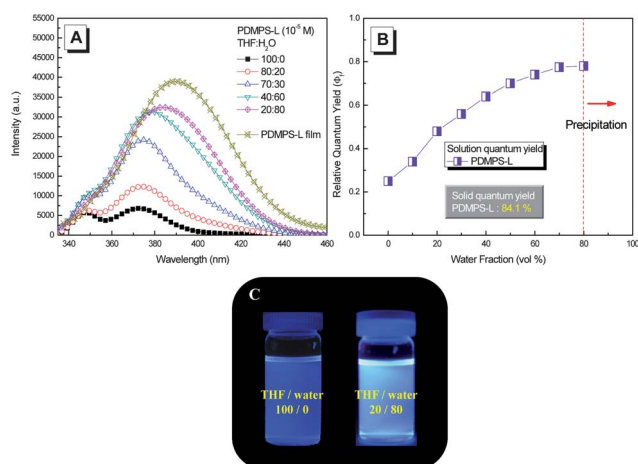


**Fig. 5** (A) FL emission spectra of solid film and dilute ( $10^{-5}$  M) solution of PDMPS-L in THF/water solvent mixtures of varied compositions, (B) the summarized solution quantum yield ( $\Phi_F$ ) vs. solution composition (inset: solid quantum yield), and (C) photographs of PDMPS-L in pure THF (left) and THF/water mixture (80% volume fraction of water) (right) under illumination with a 365 nm UV lamp.

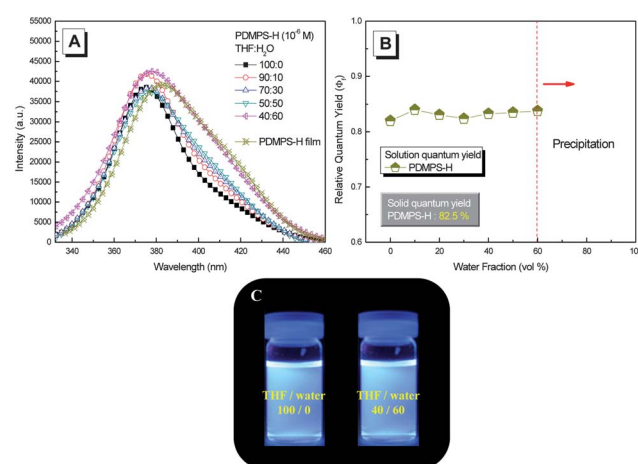


**Fig. 6** (A) FL emission spectra of solid film and dilute ( $10^{-5}$  M) solution of PDMPS-H in THF/water solvent mixtures of varied compositions, (B) the summarized quantum yield ( $\Phi_F$ ) vs. solution composition (inset: solid quantum yield), and (C) photographs of PDMPS-H in pure THF (left) and THF/water mixture (60% volume fractions of water) (right) under illumination with a 365 nm UV lamp.

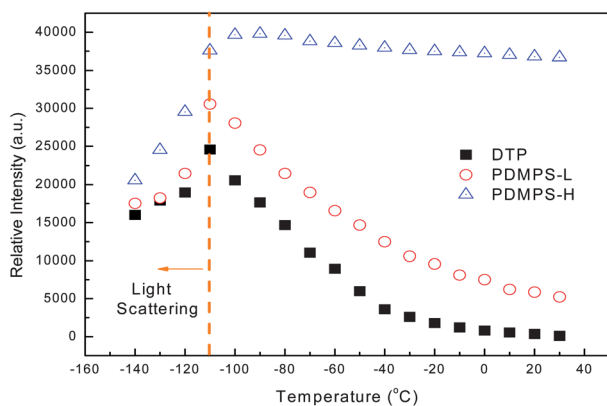


**Fig. 7** The maximum peak intensity of DTP, PDMPS-L and -H solutions ( $10^{-5}$  M) in THF at different reduced temperatures.

the frozen THF media caused the emission reductions in all three systems.

The  $^1\text{H}$  NMR spectra in Fig. 2 can be used to evaluate the relative rotation barrier between the PDMPS-H and the -L samples. The  $^1\text{H}$  NMR band shape analysis had been utilized in the studies of rotation-induced conformational changes in the AIE-active silole compounds.<sup>6</sup> It had been shown that the fast conformational exchanges caused by the fast intramolecular rotations upon the single-bond axes give sharp resonance peaks, whereas the slower exchanges due to the slow rotations broaden the resonance peaks. Dilute solution ( $10^{-3}$  M) of PDMPS-L in DMSO- $d_6$  gave the divided resonance peaks of the aromatic protons (g–k) in the ranges of 7.3–7.9 ppm, which is essentially different from the broad aromatic resonance band observed in spectrum of PDMPS-H. Other than the aromatic resonance peaks, the rest of the spectra are essentially the same for both samples, which indicated that only the molecular rotations of the TP pendant groups are strongly affected by the MW difference. The  $^1\text{H}$  NMR spectra in Fig. 2 demonstrated that the molecular rotations of the TP fluorophores in PDMPS-H are indeed restricted more seriously than the TPs in PDMPS-L.

The time-resolved fluorescence spectra were then taken to study the decay behaviors. The decay curves in Fig. 8 clearly suggest that the PDMPS-H solution has slower decay rate than the PDMPS-L solution. The resolved data from the decay curves can be quantitatively fitted with the double-exponential function of  $y = A_1e^{-t/\tau_1} + A_2e^{-t/\tau_2}$ , which suggests that the solution excited states decay through the fast and the slow pathways with the values of  $A_1$  and  $A_2$  representative of their respective fractions and  $\tau_1$  and  $\tau_2$  the respective lifetimes. Presumably, the fast-decay pathways are due to excited species in more isolated (monomer) units while the slow-decay pathways are from paired species in the aggregated regions. The summarized results in Table 2 suggest that aggregate decay pathway occupies a higher fraction of 91% for PDMPS-H as compared to a less of 63% for PDMPS-L solutions, which is consistent with the above conclusion that degree of aggregation is high for high MW PDMPS-H but low for low MW analogue. The average lifetime ( $\tau$ ) formulated from  $\tau = (A_1\tau_1 + A_2\tau_2)/(A_1 + A_2)$  is also consistent with the order of PDMPS-H > PDMPS-L (7.58 vs. 2.71 ns).

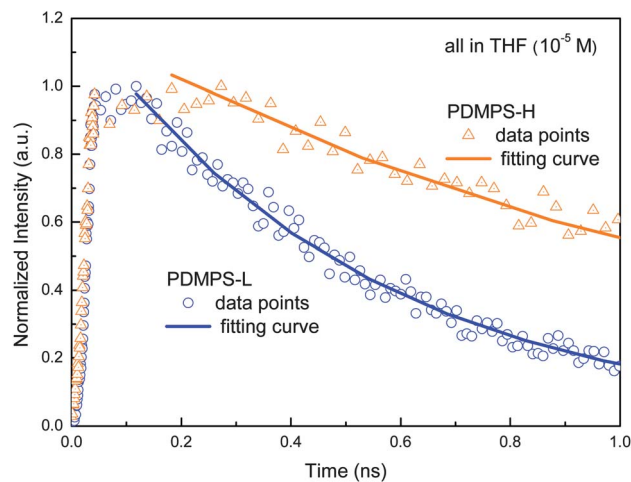


**Fig. 8** Fluorescent decay spectroscopy of PDMPS-L and -H solutions ( $10^{-5}$  M) in THF.

### Characterizations of the solid PDMPS-L and -H films

Good thermal stability of fluorescent polymers generally requires better spectral stability at high temperature and the higher  $T_g$  (211 °C) of PDMPS-H means better spectral stability of PDMPS-H when compared to PDMPS-L with a lower  $T_g$  of 160 °C. To demonstrate, the fluorescence intensity of both solid films was measured at temperatures across the respective glass transitions (Fig. 9A) and indeed, the high MW PDMPS-H showed little emission reduction even heated to temperatures beyond its  $T_g$ , which is widely different from the large emission decrease (to less than 2/3 of the original intensity) observed in the PDMPS-L sample. Both solid samples are deep-blue emitters and the PDMPS-H film emitted brightly (*cf.* the inserted photo) at a high temperature of 250 °C, which makes it particularly interesting and the advantageous spectral stability should be due to its high MW.

To demonstrate, the rheological stability of both film samples were measured at temperatures across their respective glass transitions. The complex viscosity vs. temperature plot in Fig. 9B suggests that the high MW PDMPS-H sample has much higher viscosity than the low MW PDMPS-L sample. Both samples exhibited a viscosity drop during the glass transitions; however, beyond  $T_g$ , the PDMPS-H sample still possessed a much higher viscosity than PDMPS-L ( $5.5 \times 10^4$  vs. 23 Pa s at 250 °C). It is envisaged that the numerous entangled chains across the long chain segment of the high MW PDMPS-H maintained its high viscosity in the viscous liquid state at high temperatures; in contrast, the low entangled segments in the PDMPS-L sample

**Table 2** Data calculated from the fluorescent decay curves in Fig. 8

Sample	$A_1$ (%) <sup>a</sup>	$A_2$ (%) <sup>a</sup>	$\tau_1$ (ns) <sup>a</sup>	$\tau_2$ (ns) <sup>a</sup>	$\tau$ (ns) <sup>b</sup>
PDMPS-L	37	63	0.75	3.87	2.71
PDMPS-H	9	91	0.73	8.26	7.58

<sup>a</sup> Determined from the fitting function of  $y = A_1e^{-t/\tau_1} + A_2e^{-t/\tau_2}$  from the fluorescence decay curves in Fig. 8. <sup>b</sup> Determined from  $\tau = (A_1\tau_1 + A_2\tau_2)/(A_1 + A_2)$ .

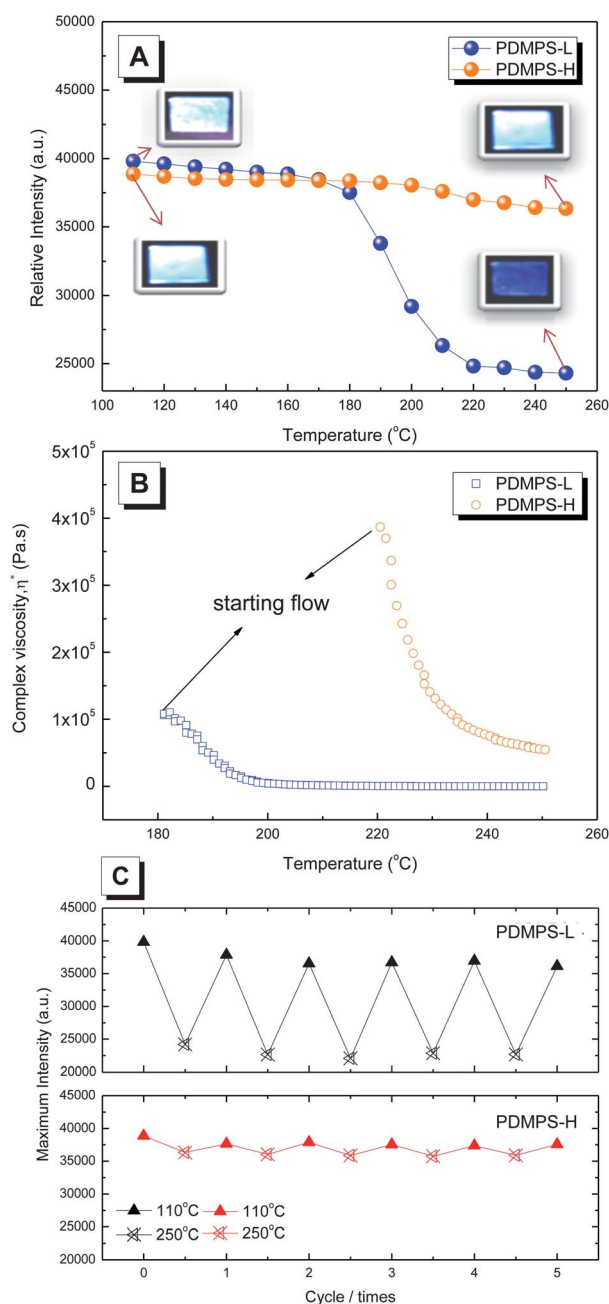


**Fig. 9** (A) Relative emission intensity and (B) rheogram of complex viscosity for samples PDMPS-L and -H films measured at high temperatures. (C) The fluorescence modulation spectrum shows the thermo-reversibility of the FL intensity (heating rate:  $2\text{ }^\circ\text{C min}^{-1}$ ).

are incapable of keeping up a reasonable viscosity to maintain mechanical integrity in the flow state. Here, the restricted molecular rotations of the TP fluorophores imposed by the entangled segments of PDMPS-H sample are supposed to function well to exert efficient AIEE-oriented emission in the viscous state; however, the low viscosity of the PDMPS-L chain at high temperatures led to large emission reduction due to the free molecular rotations of the less-entangled chains at high temperatures. The thermo-reversibility of the FL/temperature response of the PDMPS-L and -H samples can be evaluated from

their FL intensity response toward repeated heating/cooling cycles. The results shown in Fig. 9C suggest that both polymers can be reversibly heated without reducing their emission intensity. Thermal stability of the low and high MW PDMPSSs is also different. The TGA thermograms (Fig. S8, ESI<sup>†</sup>) indicate that the polymer PDMPS-H has a higher on-set decomposition temperature ( $T_D$ ) and a higher residual weight ( $W_R$ ) after heating to  $750\text{ }^\circ\text{C}$  than the PDMPS-L ( $T_D = 410$  vs.  $380\text{ }^\circ\text{C}$  and  $W_R = 51$  vs.  $27\text{ wt}\%$ ) sample.

### Theoretical approach to the single-chain conformers of PDMPS-L and -H

The single-chain conformations of the PDMPS-L and -H polymers were then studied by computer simulation from the Molecular Studio package in order to evaluate the plausible reason for their emission behavior. Primarily, the repeat unit with minimum-energy needed to be built and was used to construct the single chains with the respective 100 and 1000 repeat units representative of the low and the high MW analogues. As illustrated in Fig. 10, the resultant PDMPS-L conformer after energy-minimization (top) possesses a linear main-chain with low curvature (*cf.* the purple main-chain framework inserted in the top circle). In contrast, the resolved PDMPS-H conformer mainly contains several intersected loops connected by the highly-curved intersegments (Fig. 10, bottom). Here, we described the resultant PDMPS-H conformer as a coil-like chain for the sake of convenience. Careful inspection for the

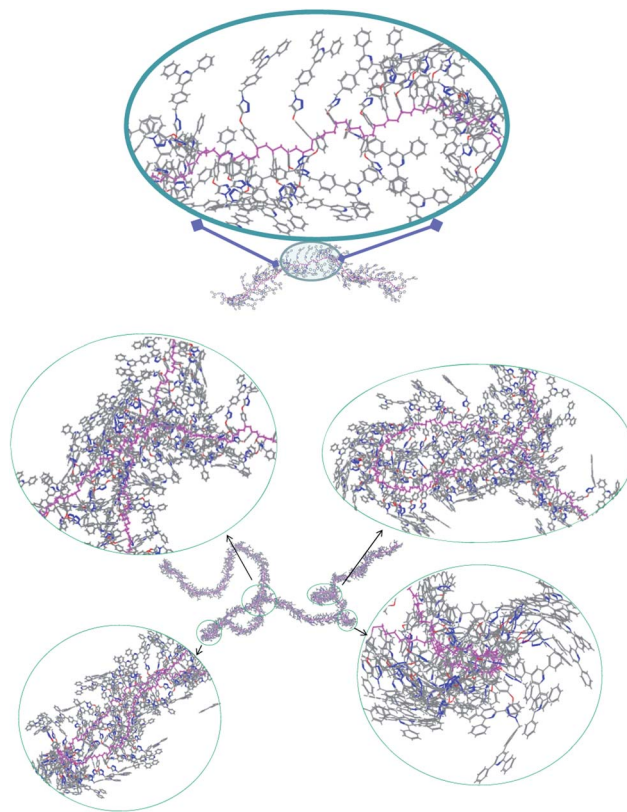


**Fig. 10** Single-chain conformers of PDMPS-L (top) and PDMPS-H (bottom) simulated from MS.

more linear PDMPS-L chain suggested that most of the fluorophoric TP units in the adjacent pendant groups are actually pointed away from each other and become spatially isolated from the vicinal TP fluorophores, which are the monomer units responsible for the weak emission in the dilute ( $10^{-5}$  M) solution of PDMPS-L due to the lack of aggregated TPs to exert AIE-operative emission. For the coil-like PDMPS-H chain, the highly-curved regions and the intersected loops contain abundant sources of intimately-packed 1,3-TP pairs, which contributed to the excimer emission upon photo-irradiating the dilute ( $10^{-5}$  M) solution of PDMPS-H in THF.

When aggregates formed in the mixture solutions, intermolecular interactions for the linear PDMPS-L and the coil-like PDMPS-H chains is schematically illustrated in Scheme 2. In the aggregated domains, the intimate contacts among the linear PDMPS-L chains proceeded readily and the densely-packing of the TP fluorophores within the compact aggregates are conceivable; thus, aggregate emission increased (*cf.* Fig. 5A) when water was included to generate aggregates containing the densely-packed fluorophores. In contrast, few intimately-contacted TP pairs can be further gained for the intermolecular approaches of the large PDMPS-H coils due to the geometrical restraint and in this case, coil aggregates with loose intermolecular contacts may be yielded. The little intermolecular association may account for the small emission variations for the different mixture solutions of PDMPS-H (*cf.* Fig. 6A). With the inclusion of water, aggregated nanoparticles with varied hydrodynamic volumes formed. The DLS analysis (Fig. S9, ESI†) on the mixture solutions suggests that the aggregated nanoparticles generated for the mixture solutions of PDMPS-H are comparatively larger than the nanoparticles formed in the PDMPS-L solutions, a result possibly correlated with the loose and the dense geometrical arrangements inside the aggregated nanoparticles of the PDMPS-H and -L solutions, respectively. With the increasing water content from 20 to 80 vol%, the average hydrodynamic diameter ( $D_h$ ) of the PDMPS-L nanoparticles evaluated from the mixture solutions decreased from 136 to 71 nm, which are much smaller than those found in the PDMPS-H solutions ( $D_h = 341\text{--}185$  nm from 10 to 60 vol% water

solutions). The volume shrinkage which occurred in the PDMPS-L solution led to the bathochromic shift of the aggregate emission and the emission enhancement observed in Fig. 5A; suggesting that the shrinkage of the aggregated nanoparticles forced the interior aromatic TP fluorophores to pack in a more coplanar fashion, which extended conjugation and the bathochromic shift of the long-wavelength aggregation emissions with increasing water inclusion. The steric crowdedness imposed by the volume shrinkage also restrains the free rotation of the aromatic rings and blocks the nonradiative decay channels, leading to the observed emission enhancements in Fig. 5A. The large aggregated particles formed in the PDMPS-H mixture solutions allows little changes of the geometrical arrangements of the 1,3-TP pairs in the aggregated states. The invariant 1,3-TP pairs responsible for the excimer emission are considered to persist in the solution, aggregate and solid states as judged by the similar emission spectra illustrated in Fig. 6A.

## Conclusions

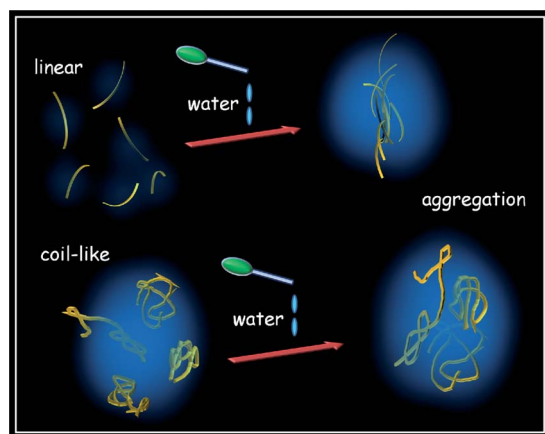
The high and low MW PDMPS-H and -L polymers with novel AIE-active TP pendant groups were successfully prepared through the facile click reaction between the azide-functionalized APDP and vinyl polymer with the acetylene pendant groups. Both the solid PDMPS-L and -H films are good deep-blue emitters with the high  $\Phi_F$  values of 84.1 and 82.5%, respectively. With high MW, the PDMPS-H polymer has a high  $T_g$  (211 °C) and enhanced spectral stability without any emission reduction after heating to temperature above 200 °C.

The simulated single-chain conformer of PDMPS-L contains linear framework with most of the pendant TP fluorophores isolated to each other, which are responsible for the weak emission in dilute solution. With the inclusion of nonsolvent water, the intimate intermolecular contacts of the linear chains facilitate formations of densely-packed TP aggregates, leading to large emission enhancement. In contrast, despite the single coil-like PDMPS-H chain containing more aggregated domains, intermolecular approaches among the coil-like chains gained little aggregated TP pairs, resulting in the constant emission intensity with further water inclusion.

## Experimental

### Materials

Reagent grade acetophenone, *p*-tolualdehyde, ammonium acetate, sodium sulfite ( $\text{Na}_2\text{SO}_3$ ), sodium azide ( $\text{NaN}_3$ ), *sec*-butyllithium solution (1.3 M in cyclohexane), 4-*tert*-butoxystyrene (BV), propargyl bromide solution (80 wt% in toluene), alumina oxide, acetic acid and dioxane were purchased from Aldrich Chemical Company and used directly without purification. Benzoyl peroxide (BPO; Acros) and *N*-bromosuccinimide (NBS; Aldrich) were recrystallized from chloroform/methanol and acetone, respectively. CuBr (98%, Aldrich) was stirred overnight in acetic acid, filtered and washed with ethanol and diethyl ether before dried in vacuo. THF was refluxed over sodium/benzophenone under nitrogen for more than 2–3 days before distillation to use. *N,N*-dimethylformamide (DMF; Aldrich) and dichloromethane (DCM; Aldrich) were refluxed over  $\text{CaH}_2$  under nitrogen for 5 h before distillation for use.



**Scheme 2** Intermolecular approaches within the aggregated nanoparticles for the more linear PDMPS-L and the coil-like PDMPS-H chains.

## Characterization

<sup>1</sup>H NMR spectra were recorded on a Varian VXR-500 MHz instrument (resonance frequency of 500 MHz) operated in the Fourier transform mode with CDCl<sub>3</sub> or (CD<sub>3</sub>)<sub>2</sub>SO as the solvent. A VG Quattro GC-MS/MS/DS instrument was used to determine the molar mass of the organic molecules. The sample was charged into rapidly moving gas and converted into ions, which can be separated based on their mass-to-charge ratios (*m/z*). Molecular weight and molecular weight distribution of polymers were determined from GPC using a Waters 510 HPLC model equipped with a 410 differential refractometer, an UV detector and three Ultrastaygel columns (100, 500, and 1000 Å) connected in series. Polymer solution was eluted by THF or DMF with a flow rate of 0.6 mL min<sup>-1</sup>. A set of monodisperse polystyrene standards covering molecular weight range of 10<sup>3</sup>–10<sup>6</sup> g mol<sup>-1</sup> was used for the molecular weight calibration. The glass transition temperatures (*T*<sub>g</sub>) of the polymers were obtained from a TA Q-20 DSC calorimeter with a scan rate of 20 °C min<sup>-1</sup>. FT-IR spectra were recorded on a Nicolet IR-200 spectrometer. Sample solution in THF was dropped on a KBr pellet and dried at 100 °C under vacuum to prepare solid samples for analysis. The UV-vis absorption spectra were recorded with an Ocean Optics DT 1000 CE 376 spectrophotometer. The FL emission spectra were obtained from a LabGuide X350 fluorescence spectrophotometer using a 450W Xe lamp as the continuous light source. Solution quantum yield ( $\Phi_F$ ) in solvent mixture of varied compositions was determined by comparison with a quinine sulfate standard solution (10<sup>-5</sup> M in 0.1 N H<sub>2</sub>SO<sub>4</sub>,  $\Phi_F = 55\%$ ). Integrating sphere was used to measure the quantum yields of the solid films. Particle sizes of polymer aggregates in solvent mixtures were analyzed by dynamic light scattering (DLS) using a Brookhaven 90 plus spectrometer equipped with a temperature controller. An argon ion laser operating at 658 nm was used as light source. The rheological behavior of the PDMPS-L and PDMPS-H were studied using TA Instruments AR 2000ex Rheometer. The experiments were operated under a fixed oscillation frequency of 10 Hz at different elevated temperatures with a scan rate of 2 °C min<sup>-1</sup>. Single-chain conformations of PDMPS polymers were formulated from the Materials Studio (MS) commercial software of Accelrys Inc. The repeat unit with the geometry optimization was primarily built by Gaussian MS Program. The polymeric chains with the respective 100 and 1000 repeat units were then constructed to represent the low and the high MW PDMPS-L and -H, respectively. The Smart Minimizer incorporated in the Discover MS Program<sup>33</sup> was used to broadcast the minimum-energy conformer of PDMPS-L and -H.

## Syntheses of small molecules and polymers

Catalyst tris(2-dimethylaminoethyl)amine (Me<sub>6</sub>-TREN)<sup>31</sup> for Click reaction was prepared by the reported procedures. Organic molecules and polymers shown in Scheme 1 were prepared according to the detailed procedures below.

**Preparation of 2,6-diphenyl-4-p-tolylpyridine (DTP).** A mixture of acetophenone (12 g, 99.87 mmol), *p*-tolualdehyde (6 g, 49.93 mmol), ammonium acetate (60 g, 0.78 mol) and acetic acid (100 mL) was heated and reacted at 115 °C for 24 h. After cooling

to 0 °C, the precipitates were filtered, washed with methanol, and dried *in vacuo* to afford pale yellow solid. After recrystallization from methanol three times, the fluffy and yellowish needle product (5.38 g, 34% yield) was obtained. IR (KBr pellet, cm<sup>-1</sup>): 3025, 2922, 2855, 1598, 1543, 1399, 1241, 1181, 1115, 1076, 1027, 877, 817, 771, 737, 692, 568. <sup>1</sup>H NMR (500 MHz, CDCl<sub>3</sub>):  $\delta$  2.45 (s, 3H, H<sub>a</sub>), 7.34 (d, 2H, H<sub>b</sub>), 7.45 (t, 2H, H<sub>c</sub>), 7.52 (t, 4H, H<sub>d</sub>), 7.66 (d, 2H, H<sub>e</sub>), 7.88 (s, 2H, H<sub>f</sub>), 8.21 (d, 4H, H<sub>g</sub>) (Fig. S1, ESI<sup>†</sup>). MS, *m/z*: calcd for C<sub>24</sub>H<sub>19</sub>N, 321.15; found, 321.04 (M<sup>+</sup>). Anal. Calcd for C<sub>24</sub>H<sub>19</sub>N: C, 89.68; H, 5.96; N, 4.36. Found: C, 89.59; H, 6.12; N, 4.28.

**Preparation of 4-(4-(bromomethyl)phenyl)-2,6-diphenylpyridine (BPDP).** Solution mixtures of DTP (4 g, 12.45 mmol), NBS (2.31 g, 13 mmol) and BPO (3.15 g, 13 mmol) in CCl<sub>4</sub> (20 mL) were stirred under nitrogen in a two-necked flask to become homogeneous before heated at 80 °C for 24 h. After cooling to room temperature, the succinimide side product was removed by filtration. Aqueous Na<sub>2</sub>SO<sub>3</sub> (~20 mL) was then added to the filtrate and the whole solution was stirred vigorously in order to reduce excess bromine. The solution was extracted with chloroform (15 mL) and washed with water (40 mL). The organic layer was collected and dried over MgSO<sub>4</sub>. All volatiles were then removed under reduced pressure. Column chromatography (hexane eluent) was applied to yield the yellow oily product (1.8 g; 36.1% yield). IR (KBr pellet, cm<sup>-1</sup>): 3061, 3033, 2955, 2926, 2854, 1599, 1546, 1451, 1421, 1392, 1229, 1204, 1179, 1073, 1025, 920, 879, 836, 774, 739, 691, 604, 504. <sup>1</sup>H NMR (500 MHz, CDCl<sub>3</sub>):  $\delta$  4.35 (s, 2H, H<sub>a</sub>), 7.34 (d, 2H, H<sub>b</sub>), 7.45 (t, 2H, H<sub>c</sub>), 7.52 (t, 4H, H<sub>d</sub>), 7.66 (d, 2H, H<sub>e</sub>), 7.88 (s, 2H, H<sub>f</sub>), 8.21 (d, 4H, H<sub>g</sub>) (Fig. S2, ESI<sup>†</sup>). MS, *m/z*: calcd for C<sub>24</sub>H<sub>18</sub>BrN, 399.06; found, 399.29 (M<sup>+</sup>). Anal. Calcd for C<sub>24</sub>H<sub>18</sub>BrN: C, 72.01; H, 4.53; Br, 19.96; N, 3.50. Found: C, 72.30; H, 4.00; Br, 20.21; N, 3.48.

**Preparation of 4-(4-(azidomethyl)phenyl)-2,6-diphenylpyridine (APDP).** Suspension of BPDP (1 g, 2.5 mmol) and NaN<sub>3</sub> (0.2 g, 3 mmol) in DMF (20 mL) was heated at 80 °C for 24 h. Excess solvent was then removed by vacuum distillation at elevated temperature. The resultant solid was dissolved in 30 mL dichloromethane and washed with 150 mL of saturated aq. NaCl solution twice. The organic layer was then dried over MgSO<sub>4</sub> before concentrated to obtain crude mixture. Final product (0.1 g; 11% yield) was obtained after column chromatography (hexane eluent). IR (KBr pellet, cm<sup>-1</sup>): 3061, 3035, 2958, 2925, 2851, 2099, 1596, 1543, 1391, 1247, 1185, 1078, 1025, 835, 769, 737, 691 (Fig. S4, ESI<sup>†</sup>). <sup>1</sup>H NMR (500 MHz, CDCl<sub>3</sub>):  $\delta$  4.24 (s, 2H, H<sub>a</sub>), 7.34 (d, 2H, H<sub>b</sub>), 7.45 (t, 2H, H<sub>c</sub>), 7.52 (t, 4H, H<sub>d</sub>), 7.66 (d, 2H, H<sub>e</sub>), 7.88 (s, 2H, H<sub>f</sub>), 8.21 (d, 4H, H<sub>g</sub>) (Fig. S3, ESI<sup>†</sup>). MS, *m/z*: calcd for C<sub>24</sub>H<sub>18</sub>N<sub>4</sub>, 362.15; found, 362.11 (M<sup>+</sup>). Anal. Calcd for C<sub>24</sub>H<sub>18</sub>N<sub>4</sub>: C, 79.54; H, 5.01; N, 15.46. Found: C, 79.81; H, 4.69; N, 15.49.

**Preparation of PBS-L and -H by anionic polymerization.** A PBS-L polymer was synthesized by living anionic polymerization under an inert atmosphere in THF (500 mL) using *sec*-butyllithium (0.22 mL, 0.28 mmol; 1.3 M in cyclohexane) as the initiator at -78 °C. The 4-*tert*-butoxystyrene (BV; 5 g) monomer was then injected *via* syringe and polymerization was allowed to proceed at -78 °C for 2 h before warmed up to room

temperature and terminated with methanol. The solid precipitates were filtered and washed with methanol three times before vacuum drying to yield the final polymer as blond yellow powder (4.5 g; 90% yield). The synthesis of PBS-H was operated with the same procedures as for PBS-L but different recipes (*sec*-butyllithium = 0.02 ml (0.026 mmol) and BV = 5 g) was used. PBS-L:  $T_g = 96\text{ }^\circ\text{C}$  (Fig. 3). IR (KBr pellet,  $\text{cm}^{-1}$ ) 2976, 2927, 1604, 1502, 1446, 1239, 1165, 895, 848, 550.  $^1\text{H}$  NMR (500 MHz,  $\text{CDCl}_3$ ):  $\delta$  0.55–2.48 (b, 12H,  $\text{H}_a$ ,  $\text{H}_b$ ,  $\text{H}_c$ ), 5.91–6.44 (b, 2H,  $\text{H}_d$ ), 6.45–6.86 (b, 2H,  $\text{H}_e$ ) (Fig. 1). PBS-H:  $T_g = 114\text{ }^\circ\text{C}$  (Fig. 3). IR (KBr pellet,  $\text{cm}^{-1}$ ) 2976, 2927, 1606, 1505, 1455, 1377, 1242, 1167, 900, 853.  $^1\text{H}$  NMR (500 MHz,  $\text{CDCl}_3$ ):  $\delta$  0.55–2.54 (b, 12H,  $\text{H}_a$ ,  $\text{H}_b$ ,  $\text{H}_c$ ), 5.96–6.89 (b, 4H,  $\text{H}_d$ ,  $\text{H}_e$ ) (Fig. 1).

**Preparation of PVPh-L and -H.** Hydrolysis of polymer PBS afforded the desired poly(4-vinylphenol) (PVPh). The PBS-L (3.5 g, 19.86 mmol) was dissolved in dioxane (50 mL) before the introduction of aq. HCl (37 wt%, 2 mL) solution. The mixture was stirred at  $80\text{ }^\circ\text{C}$  overnight and the resultant product was precipitated from methanol/water (v/v = 2/8) mixture. After neutralization with aq. NaOH (10 wt%) solution, the resultant product was filtered off. Repeated dissolution and precipitation by THF and methanol/water solvents were then conducted to yield crude product for further Soxhlet extraction with water for 3 days. Final products of PVPh-L (2.1 g, 88%) and -H (2.25 g, 94% yield) were obtained after vacuum drying at  $80\text{ }^\circ\text{C}$ . PVPh-L:  $T_g = 156\text{ }^\circ\text{C}$  (Fig. 3). IR (KBr pellet,  $\text{cm}^{-1}$ ) 3689–3072, 3021, 2921, 2847, 1607, 1514, 1445, 1364, 1229, 1168, 1104, 1013, 828, 552 (Fig. S4A, ESI $^\dagger$ ).  $^1\text{H}$  NMR (500 MHz,  $\text{CDCl}_3$ ):  $\delta$  0.88–2.11 (b, 3H,  $\text{H}_a$ ,  $\text{H}_b$ ), 6.09–6.74 (b, 4H,  $\text{H}_c$ ,  $\text{H}_d$ ), 8.85–9.20 (b, 1H,  $\text{H}_e$ ) (Fig. 1). PVPh-H:  $T_g = 191\text{ }^\circ\text{C}$  (Fig. 3). IR (KBr pellet,  $\text{cm}^{-1}$ ) 3687–3083, 3022, 2921, 2847, 1606, 1512, 1443, 1361, 1230, 1173, 1108, 828, 545 (Fig. S4B, ESI $^\dagger$ ).  $^1\text{H}$  NMR (500 MHz,  $\text{CDCl}_3$ ):  $\delta$  0.77–2.22 (b, 3H,  $\text{H}_a$ ,  $\text{H}_b$ ), 5.88–6.96 (b, 4H,  $\text{H}_c$ ,  $\text{H}_d$ ), 8.72–9.27 (b, 1H,  $\text{H}_e$ ) (Fig. 1).

**Preparation of PPS-L and -H.** Propargyl bromide (1.78 g, 15 mmol) was added to a mixture of PVPh-L (1.5 g, 12.48 mmol) and  $\text{K}_2\text{CO}_3$  (2.07 g, 15 mmol) in dry DMF (40 mL) and stirred at  $65\text{ }^\circ\text{C}$  for 24 h under nitrogen atmosphere. The resultant mixtures were precipitated by methanol/water (v/v = 5/5) and the precipitate was filtered and dried under vacuum at  $80\text{ }^\circ\text{C}$  to obtain PPS-L (1.87 g, 95% yield). The synthesis of PPS-H (1.63 g, 83% yield) followed the same procedures. PPS-L:  $T_g = 64\text{ }^\circ\text{C}$  (Fig. 3). IR (KBr pellet,  $\text{cm}^{-1}$ ) 3290, 3030, 2924, 2856, 1609, 1581, 1511, 1452, 1373, 1304, 1264, 1220, 1178, 1114, 1032, 923, 826, 681, 646, 554 (Fig. S4A, ESI $^\dagger$ ).  $^1\text{H}$  NMR (500 MHz,  $\text{CDCl}_3$ ):  $\delta$  0.34–2.25 (b, 3H,  $\text{H}_a$ ,  $\text{H}_b$ ), 3.37–3.59 (b, 1H,  $\text{H}_c$ ), 4.57–4.80 (b, 2H,  $\text{H}_d$ ), 6.21–7.06 (b, 4H,  $\text{H}_e$ ,  $\text{H}_f$ ) (Fig. 1). PPS-H:  $T_g = 83\text{ }^\circ\text{C}$  (Fig. 3). IR (KBr pellet,  $\text{cm}^{-1}$ ) 3289, 3034, 2924, 2858, 1609, 1508, 1451, 1372, 1300, 1225, 1180, 1114, 1029, 925, 831, 679, 647, 552 (Fig. S4B, ESI $^\dagger$ ).  $^1\text{H}$  NMR (500 MHz,  $\text{CDCl}_3$ ):  $\delta$  0.32–2.27 (b, 3H,  $\text{H}_a$ ,  $\text{H}_b$ ), 3.36–3.62 (b, 1H,  $\text{H}_c$ ), 4.48–4.88 (b, 2H,  $\text{H}_d$ ), 6.05–7.21 (b, 4H,  $\text{H}_e$ ,  $\text{H}_f$ ) (Fig. 1).

**Preparations of PDMPS-L and -H (click reaction).** A typical procedure for the click reaction is as follows: DMF (10 mL) was placed in a three-neck flask and degassed by bubbling argon gas for 1.5 h before the addition of CuBr (20 mg, 0.14 mmol), APDP

(0.25 g, 0.69 mmol) and PPS-L (0.1 g, 0.69 mmol). A solution of  $\text{Me}_6\text{-TREN}$  (46 mg; 0.2 mmol) in degassed DMF (5 mL) was then introduced and the resultant transparent solution was heated at  $80\text{ }^\circ\text{C}$  under argon atmosphere for 48 h. When the mixture was cooled to room temperature, DMF was distilled off under reduced pressure. The residue was then diluted with THF before passing through an alumina column to remove the copper catalyst. The solid product was then precipitated from methanol. Subsequent dissolution/precipitation procedures by THF/methanol (v/v = 1.5/8.5) were repeated twice before vacuum drying to yield the final polymer as yellow powder (PDMPS-L, 0.34 g, 95% yield). The synthesis of PDMPS-H (0.315 g, 88% yield) followed the same procedures. PDMPS-L:  $T_g = 160\text{ }^\circ\text{C}$  (Fig. 3). IR (KBr pellet,  $\text{cm}^{-1}$ ) 3059, 3034, 2922, 2852, 1600, 1543, 1503, 1454, 1394, 1226, 1031, 832, 775, 699 (Fig. S4A, ESI $^\dagger$ ).  $^1\text{H}$  NMR (500 MHz,  $\text{CDCl}_3$ ):  $\delta$  0.40–2.28 (b, 3H,  $\text{H}_a$ ,  $\text{H}_b$ ), 5.01–5.23 (b, 2H,  $\text{H}_c$ ), 5.50–5.70 (b, 2H,  $\text{H}_d$ ), 6.23–6.93 (b, 4H,  $\text{H}_e$ ,  $\text{H}_f$ ) 7.28–7.40 (b, 2H,  $\text{H}_g$ ) 7.40–7.60 (b, 6H,  $\text{H}_h$ ,  $\text{H}_i$ ) 7.60–7.75 (b, 2H,  $\text{H}_j$ ) 7.81–7.95 (b, 2H,  $\text{H}_k$ ) 8.12–8.36 (b, 5H,  $\text{H}_l$ ,  $\text{H}_m$ ) (Fig. 2). PDMPS-H:  $T_g = 211\text{ }^\circ\text{C}$  (Fig. 3). IR (KBr pellet,  $\text{cm}^{-1}$ ) 3057, 3034, 2922, 2855, 1600, 1545, 1509, 1456, 1394, 1224, 1028, 828, 775, 694 (Fig. S4B, ESI $^\dagger$ ).  $^1\text{H}$  NMR (500 MHz,  $\text{CDCl}_3$ ):  $\delta$  0.39–2.30 (b, 3H,  $\text{H}_a$ ,  $\text{H}_b$ ), 4.97–5.27 (b, 2H,  $\text{H}_c$ ), 5.42–5.77 (b, 2H,  $\text{H}_d$ ), 6.15–7.03 (b, 4H,  $\text{H}_e$ ,  $\text{H}_f$ ) 7.03–8.01 (b, 12H,  $\text{H}_g$ ,  $\text{H}_h$ ,  $\text{H}_i$ ,  $\text{H}_j$ ,  $\text{H}_k$ ) 8.01–8.44 (b, 5H,  $\text{H}_l$ ,  $\text{H}_m$ ) (Fig. 2).

## Acknowledgements

We appreciate the financial support from the National Science Council, Taiwan, Republic of China, under Contract No. NSC 100-2221-E-110-045.

## Notes and references

- S. W. Thomas III, G. D. Joly and T. M. Swager, *Chem. Rev.*, 2007, **107**, 1339.
- A. Dreuw, J. Plöner, L. Lorenz, J. Wachtveitl, J. E. Djanhan, J. Brüning, T. Metz, M. Bolte and M. U. Schmidt, *Angew. Chem., Int. Ed.*, 2005, **44**, 7783.
- C.-T. Chen, *Chem. Mater.*, 2004, **16**, 4389.
- G. Qian, Z. Zhong, M. Luo, D. Yu, Z. Zhang, Z. Y. Wang and D. Ma, *Adv. Mater.*, 2009, **21**, 111.
- J. Z. Xie, J. W. Y. Lam, L. Cheng, H. Chen, C. Qiu, H. S. Kwok, X. Zhan, Y. Liu, D. Zhu and B. Z. Tang, *Chem. Commun.*, 2001, 1740.
- J. Chen, C. C. W. Law, J. W. Y. Lam, Y. Dong, S. M. F. Lo, I. D. Williams, D. Zhu and B. Z. Tang, *Chem. Mater.*, 2003, **15**, 1535.
- H. J. Tracy, J. L. Mullin, W. T. Klooster, J. A. Martin, J. Haug, S. Wallace, I. Rudloe and K. Watts, *Inorg. Chem.*, 2005, **44**, 2003.
- Z. Li, Y. Q. Dong, J. W. Y. Lam, J. Sun, A. Qin, M. Häußler, Y. P. Dong, H. H. Y. Sung, I. D. Williams, H. S. Kwok and B. Z. Tang, *Adv. Funct. Mater.*, 2009, **19**, 905.
- Y. Hong, J. W. Y. Lama and B. Z. Tang, *Chem. Commun.*, 2009, 4332.
- H. Li, Z. Chi, B. Xu, X. Zhang, X. Li, S. Liu, Y. Zhang and J. Xu, *J. Mater. Chem.*, 2011, **21**, 3760.
- T. He, X. T. Tao, J. X. Yang, D. Guo, H. B. Xia, J. Jia and M. H. Jiang, *Chem. Commun.*, 2011, **47**, 2907.
- B. Xu, Z. Chi, Z. Yang, J. Chen, S. Deng, H. Li, X. Li, Y. Zhang, N. Xu and J. Xu, *J. Mater. Chem.*, 2010, **20**, 4135.
- Z. Zhao, S. Chen, J. W. Y. Lam, P. Lu, Y. Zhong, K. S. Wong, H. S. Kwok and B. Z. Tang, *Chem. Commun.*, 2010, **46**, 2221.
- W. Wang, T. Lin, M. Wang, T. X. Liu, L. Ren, D. Chen and S. Huang, *J. Phys. Chem. B*, 2010, **114**, 5983.
- W. Z. Yuan, P. Lu, S. Chen, J. W. Y. Lam, Z. Wang, Y. Liu, H. S. Kwok, Y. Ma and B. Z. Tang, *Adv. Mater.*, 2010, **22**, 1.

- 16 W. C. Wu, C. Y. Chen, Y. Tian, S. H. Jang, Y. Hong, Y. Liu, R. Hu, B. Z. Tang, Y. T. Lee, C. T. Chen, W. C. Chen and A. K. Y. Jen, *Adv. Funct. Mater.*, 2010, **20**, 1413.
- 17 P. P. Kapadia, J. C. Widen, M. A. Magnus, D. C. Swenson and F. C. Pigge, *Tetrahedron Lett.*, 2011, **52**, 2519.
- 18 D. S. An, B. K. Lee, J. S. Lee, Y. S. Park, H. S. Song and S. Y. Park, *J. Am. Chem. Soc.*, 2004, **126**, 10232.
- 19 Z. Zhao, P. Lu, J. W. Y. Lam, Z. Wang, C. Y. K. Chan, H. H. Y. Sung, I. D. Williams, Y. Ma and B. Z. Tang, *Chem. Sci.*, 2011, **2**, 672.
- 20 J. Wang, J. Mei, W. Yuan, P. Lu, A. Qin, J. Sun, Y. Ma and B. Z. Tang, *J. Mater. Chem.*, 2011, **21**, 4056.
- 21 Y. Liu, C. Deng, L. Tang, A. Qin, R. Hu, J. Z. Sun and B. Z. Tang, *J. Am. Chem. Soc.*, 2011, **133**, 660.
- 22 P. S. Salini, A. P. Thomas, R. Sabarinathan, S. Ramakrishnan, K. C. G. Sreedevi, M. L. P. Reddy and A. Srinivasan, *Chem.–Eur. J.*, 2011, **17**, 6598.
- 23 X. Zhang, Z. Chi, H. Li, B. Xu, X. Li, S. Liu, Y. Zhang and J. Xu, *J. Mater. Chem.*, 2011, **21**, 1788.
- 24 B. Wang, Y. Wang, J. Hua, Y. Jiang, J. Huang, S. Qian and H. Tian, *Chem.–Eur. J.*, 2011, **17**, 2647.
- 25 Z. Zhao, D. Liu, F. Mahtab, L. Xin, Z. Shen, Y. Yu, C. Y. K. Chan, P. Lu, J. W. Y. Lam, H. H. Y. Sung, I. D. Williams, B. Yang, Y. Ma and B. Z. Tang, *Chem.–Eur. J.*, 2011, **17**, 5998.
- 26 A. Pérez, J. L. Serrano, T. Sierra, A. Ballesteros, D. d. Saá and J. Barluenga, *J. Am. Chem. Soc.*, 2011, **133**, 8110.
- 27 T. L. Bandrowsky, J. B. Carroll and J. B. Wilking, *Organometallics*, 2011, **30**, 3559.
- 28 H. H. Lin, Y. C. Chan, J. W. Chen and C. C. Chang, *J. Mater. Chem.*, 2011, **21**, 3170.
- 29 K. Kokado and Y. Chujo, *Macromolecules*, 2009, **42**, 1418.
- 30 R. H. Chien, C. T. Lai and J. L. Hong, *J. Phys. Chem. C*, 2011, **115**, 5958.
- 31 C. T. Lai, R. H. Chien, S. W. Kuo and J. L. Hong, *Macromolecules*, 2011, **44**, 6546.
- 32 J. Liu, Y. Zhong, J. W. Y. Lam, P. Lu, Y. Hong, Y. Yu, Y. Yue, M. Faisal, H. H. Y. Sung, I. D. Williams, K. S. Wong and B. Z. Tang, *Macromolecules*, 2010, **43**, 4921.
- 33 C. T. Lai and J. L. Hong, *J. Phys. Chem. B*, 2010, **114**, 10302.
- 34 A. Qin, J. W. Y. Lam, L. Tang, C. K. W. Jim, H. Zhao, J. Sun and B. Z. Tang, *Macromolecules*, 2009, **42**, 1421.
- 35 W. Z. Yuan, A. Qin, J. W. Y. Lam, J. Z. Sun, Y. Dong, M. Häussler, J. Liu, H. P. Xu, Q. Zheng and B. Z. Tang, *Macromolecules*, 2007, **40**, 3159.
- 36 R. H. Chien, C. T. Lai and J. L. Hong, *J. Phys. Chem. C*, 2011, **115**, 12358.
- 37 B. Xu, X. Wu, H. Li, H. Tong and L. Wang, *Macromolecules*, 2011, **44**, 5089.
- 38 R. H. Chien, C. T. Lai and J. L. Hong, *J. Phys. Chem. C*, 2011, **115**, 20732.
- 39 W. Z. Yuan, Z. Q. Yu, Y. Tang, J. W. Y. Lam, N. Xie, P. Lu, E. Q. Chen and B. Z. Tang, *Macromolecules*, 2011, **44**, 9618.
- 40 K. Koynov, A. Bahtiar, T. Ahn, C. Bubeck and H. –H. Hörhold, *Appl. Phys. Lett.*, 2004, **84**, 3792.
- 41 S. Shaked, S. Tal, Y. Roichman, A. Razin, S. Xiao, Y. Eichen and N. Tessler, *Adv. Mater.*, 2003, **15**, 913.
- 42 R. Traiphol, R. Potai, N. Charoenthai, T. Sriksirin, T. Kerdcharoen and T. Osotchan, *J. Polym. Sci., Part B: Polym. Phys.*, 2010, **48**, 894.
- 43 K. Koynov, A. Bahtiar, T. Ahn, R. M. Cordeiro, H. –H. Hörhold and C. Bubeck, *Macromolecules*, 2006, **39**, 8692.
- 44 D. Grando, G. P. Banfi, D. Fortusini, R. Ricceri and S. Sottini, *Synth. Met.*, 2003, **139**, 863.
- 45 R. J. Kline, M. D. McGehee, E. N. Kadnikova, J. Liu and J. M. J. Frechet, *Adv. Mater.*, 2003, **15**, 1519.
- 46 A. Zen, J. Pflaum, S. Hirschmann, W. Zhuang, F. Jaiser, U. Asawapirom, J. P. Rabe, U. Scherf and D. Neher, *Adv. Funct. Mater.*, 2004, **14**, 757.
- 47 A. Zen, M. Saphiannikova, D. Neher, J. Grenzer, S. Grigorian, U. Pietsch, U. Asawapirom, S. Janietz, U. Scherf, I. Lieberwirth and G. Wegner, *Macromolecules*, 2006, **39**, 2162.
- 48 C. Donley, J. Zaumseil, J. Andreasen, M. Nielsen, H. Sirringhaus, R. Friend and J. Kim, *J. Am. Chem. Soc.*, 2005, **127**, 12890.
- 49 M. Knaapila, B. P. Lyons, T. P. A. Hase, C. Pearson, M. C. Petty, L. Bouchenoire, P. Thompson, R. Serimaa, M. Torkkeli and A. P. Monkman, *Adv. Funct. Mater.*, 2005, **15**, 1517.
- 50 M. Knaapila, R. Stepanyan, B. P. Lyons, M. Torkkeli, T. P. A. Hase, R. Serimaa, R. Güntner, O. H. Seeck, U. Scherf and A. P. Monkman, *Macromolecules*, 2005, **38**, 2744.
- 51 K. Hosoi, T. Mori, T. Mizutani, T. Yamamoto and N. Kitamura, *Thin Solid Films*, 2003, **438–439**, 201.
- 52 A. D. Thomsen, E. Malmström and S. Hvilsted, *J. Polym. Sci., Part A: Polym. Chem.*, 2006, **44**, 6360.
- 53 V. V. Rostovtsev, L. G. Green, V. V. Fokin and K. B. Sharpless, *Angew. Chem., Int. Ed.*, 2002, **41**, 2596.
- 54 C. W. Tornøe, C. Christensen and M. Meldal, *J. Org. Chem.*, 2002, **67**, 3057.
- 55 Z. Zhao, S. Chen, J. W. Y. Lam, Z. Wang, P. Lu, F. Mahtab, H. H. Y. Sung, I. D. Williams, Y. Ma, H. S. Kwok and B. Z. Tang, *J. Mater. Chem.*, 2011, **21**, 7210.